Science of the Total Environment 444 (2013) 327–335

Contents lists available at SciVerse ScienceDirect

Science of the Total Environment

journal homepage: www.elsevier.com/locate/scitotenv

Source apportionment of PM_{10} and $PM_{2.5}$ in a desert region in northern Chile

Héctor Jorquera *, Francisco Barraza

Departmento de Ingeniería Química y Bioprocesos, Pontificia Universidad Católica de Chile, Avda. Vicuña Mackenna 4860, Santiago 6904411, Chile

HIGHLIGHTS

- Ambient PM_{10} and $PM_{2.5}$ were measured in an industrial zone within an arid region in South America.
- Dry climate allows accumulation of heavy metals deposited on the ground.
- Soil dust becomes enriched with tracers of anthropogenic activities.
- Average suspended soil dust reaches 9 μg/m^3 for $PM_{2.5}$ and 50 μg/m^3 for PM_{10}.
- Peak daily soil dust reaches 31.5 μg/m^3 for $PM_{2.5}$ and 104 μg/m^3 for PM_{10}.

ARTICLE INFO

Article history:
Received 31 August 2012
Received in revised form 7 November 2012
Accepted 3 December 2012
Available online 29 December 2012

Keywords:
Arid region
Positive matrix factorization
Natural background
Copper smelter
Cement kiln

ABSTRACT

Estimating contributions of anthropogenic sources to ambient particulate matter (PM) in desert regions is a challenging issue because wind erosion contributions are ubiquitous, significant and difficult to quantify by using source-oriented, dispersion models. A receptor modeling analysis has been applied to ambient PM_{10} and $PM_{2.5}$ measured in an industrial zone ~20 km SE of Antofagasta (23.63°S, 70.39°W), a midsize coastal city in northern Chile; the monitoring site is within a desert region that extends from northern Chile to southern Perú. Integrated 24-hour ambient samples of PM_{10} and $PM_{2.5}$ were taken with Harvard Impactors; samples were analyzed by X Ray Fluorescence, ionic chromatography (NO_3^- and $SO_4^=$), atomic absorption (Na^+, K^+) and thermal optical transmission for elemental and organic carbon determination. Receptor modeling was carried out using Positive Matrix Factorization (US EPA Version 3.0); sources were identified by looking at specific tracers, tracer ratios, local winds and wind trajectories computed from NOAA's HYSPLIT model.
For the $PM_{2.5}$ fraction, six contributions were found — cement plant, 33.7 ± 1.3%; soil dust, 22.4 ± 1.6%; sulfates, 17.8 ± 1.7%; mineral stockpiles and brine plant, 12.4 ± 1.2%; Antofagasta, 8.5 ± 1.3% and copper smelter, 5.3 ± 0.8%. For the PM_{10} fraction five sources were identified — cement plant, 38.2 ± 1.5%; soil dust, 31.2 ± 2.3%; mineral stockpiles and brine plant, 12.7 ± 1.7%; copper smelter, 11.5 ± 1.6% and marine aerosol, 6.5 ± 2.4%. Therefore local sources contribute to ambient PM concentrations more than distant sources (Antofagasta, marine aerosol) do. Soil dust is enriched with deposition of marine aerosol and calcium, sulfates and heavy metals from surrounding industrial activities. The mean contribution of suspended soil dust to PM_{10} is 50 μg/m^3 and the peak daily value is 104 μg/m^3. For the $PM_{2.5}$ fraction, suspended soil dust contributes with an average of 9.3 μg/m^3 and a peak daily value of 31.5 μg/m^3.

1. Introduction

Chile's economy is based mainly on mineral, agricultural, forest and marine exports, with primary copper and refined copper production accounting for 34% and 17% — respectively — of worldwide production in 2010 (COCHILCO, 2012). The northernmost part of Chile, from ~30°S up to the border with Perú is where most mining activities are concentrated. Source apportionment and chemical characterization of ambient particles have been reported at three coastal cities in that region. Kavouras et al. (2001) found that at Iquique (20°12′S, 70°10′W) marine aerosol contributes 40% of PM_{10} mass, but only 4.5% of $PM_{2.5}$ fraction; soil dust was a significant contribution there with 14% of PM_{10} mass but it was not found in the fine fraction. Fiebig-Wittmaack et al. (2006) found that at La Serena (29°54′S, 71°15′W) sea salt contributes 40 to 50% of the coarse particles, depending on season of the year, and that concentration decreases as the measurement site moves inland, being 10 times lower at 60 km off the coast. Jorquera (2009) found at Tocopilla (22°05′S, 70°12′W) that 50% of $PM_{2.5}$ is from sulfates originated from coal-fired thermal power plant emissions, and that marine aerosol and soil dust accounted for 35% and 15% of PM_{10}, respectively, in agreement with the results of Kavouras et al. (2001) obtained at Iquique.

The subject of the present analysis is an industrial area that has not been studied before. This industrial zone — with a cement manufacturing facility, a copper smelter, an area of minerals stockpiles

* Corresponding author. Tel.: +56 2 354 4421; fax: +56 2 354 5803.
E-mail address: jorquera@ing.puc.cl (H. Jorquera).

0048-9697/$ – see front matter © 2012 Elsevier B.V. All rights reserved.
http://dx.doi.org/10.1016/j.scitotenv.2012.12.007

and a Li_2CO_3/KCl brine extraction plant among other sources — is located SE from Antofagasta (23.63°S, 70.39°W, population: 360,000 inhabitants in 2009) on the west side of a coastal range — see Fig. 1, Supplementary material. The landscape is a desert that includes northern Chile and most of southwestern Perú — from 5°S to 30°S; in both countries mining activities have been on the rise in the last two decades, leading the economic growth in those countries.

In this study region local meteorological variables have low seasonality — see Fig. 2, Supplementary material for a long term record at Antofagasta's airport. There is a permanent stratus cloud deck which is distinctive of the South American west coast (Xu et al., 2005; Mansbach and Norris, 2007; Sun et al., 2010).

A small seasonality is present in ambient daily PM_{10} concentrations measured at the industrial site every third day with high volume samplers (SINCA, 2012) — see Fig. 3, Supplementary material. Annual PM_{10} concentrations exceed the ambient standard of 50 μg/m^3 and in all years ~25% of measured days exceed the ambient standard of 150 μg/m^3. The small seasonality in ambient PM_{10} implies that a short term campaign can capture major features of PM_{10} and $PM_{2.5}$ in that region.

At the industrial site, top hourly wind speed values exceed 5 m/s every day so wind gusts may be even larger thus contributing to wind erosion — see Fig. 4, Supplementary material for data collected during the measurement campaign. Wind erosion is ubiquitous in desert landscapes and this PM emission is difficult to estimate. Remote sensing of dust plumes is hampered by the permanent cloudiness on this coastal region. Furthermore, even under clear sky conditions, small plumes of diffuse sources are not detected by remote sensing yet they may have a substantial contribution to total dust concentrations for they cover larger areas than stronger dust sources do (Okin et al., 2011). Therefore, source-oriented dispersion models — or inverse modeling using satellite retrievals — may not estimate the total amount of naturally suspended dust in arid regions like the one analyzed herein.

In this work we report results of a short term ambient monitoring campaign of PM_{10} and $PM_{2.5}$, followed by chemical analyses for trace elements and some ions and thermal determination of organic (OC) and elemental carbon (EC). The resulting database was analyzed using EPA's PMF3 receptor model to identify and quantify major sources contributing to ambient PM concentrations. The following sections of this paper present a description of the ambient monitoring campaign, the receptor modeling approach, the results of the analysis, a discussion and a closing section with conclusions.

2. Methodology

2.1. Sampling and analytical techniques

The campaign was carried out between December 17th, 2007 and January 20th 2008 — see Fig. 1 for the location of the monitoring site. Since on Sunday December 23rd a sampling was lost, a make-up sample was taken on January 27th, also a Sunday. A total of 35 daily samples of PM_{10} and $PM_{2.5}$ were taken using low volume Harvard Impactors (Air Diagnostics and Engineering, Inc. Naples, Maine, USA) operating at a constant air flow of 10 L/min; Teflon filters (2 and 3 μm pore size, Gelman Scientific, Ann Arbor, MI, USA) were used to collect both PM size fractions; the Teflon filters were analyzed for elemental composition using X ray fluorescence, for NO_3^- and $SO_4^=$ in $PM_{2.5}$ using ionic chromatography and for Na^+ and K^+ in PM_{10} using atomic absorption. In addition, quartz fiber filters (#2500 QAT-UP, Gelman Scientific, Ann Arbor, MI, USA) were used for co-located samples of $PM_{2.5}$ that were analyzed with a DRI Model 2001 Thermal Optical Analyzer (Atmoslytic Inc., Calabasas, CA, USA) to measure elemental (EC) and organic (OC) carbon; field blank filters were also included in the sampling protocol. All chemical analyses were performed at the Desert Research Institute, Reno, NV, USA. For more details see Jorquera (2009).

2.2. Receptor modeling analysis for particulate matter

Receptor models attempt to identify and quantify sources that contribute to ambient PM concentrations at a given monitoring (receptor) site. Required data are the concentrations of n chemical species measured in m PM samples. Models explain the observed species concentrations as a sum of p source contributions (Hopke et al., 2005):

$$X_{ij} = \sum_{k=1}^{p} g_{ik} f_{kj} + e_{ij}. \quad (1)$$

In the above equation X_{ij} is the j-th species mass measured in the i-th PM sample, g_{ik} is the PM mass concentration from the k-th source

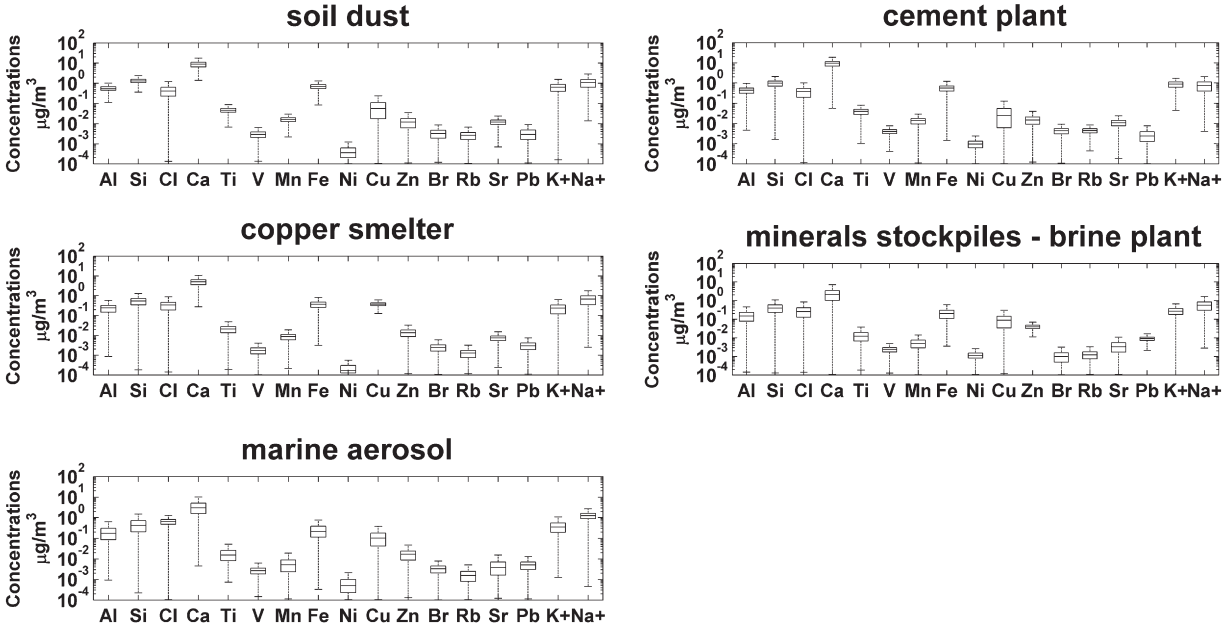

Fig. 1. Source profile concentrations [μg/m^3] for the five factor solution for ambient PM_{10} (*Fpeak* = 0).

contributing to the *i-th* PM sample, f_{kj} is the *j-th* species mass fraction from the *k-th* source, e_{ij} is a model residual and p is the total number of resolved sources. It is assumed that source profiles $\{f_{kj}\}$ are constant during the sampling period. Usually five to six sources are identified using this methodology and receptor models require a substantial amount of data points to achieve a robust source apportionment — see Pant and Harrison (2012) for a recent review.

We use in this work the software Positive Matrix Factorization (PMF, version 3.0), available from U.S. EPA (2012); this software minimizes the weighted sum of squares

$$Q = \sum_{i=1}^{n}\sum_{j=1}^{m}\left[\left(X_{ij} - \sum_{k=1}^{p} g_{ik} f_{kj}\right)/\sigma_{ij}\right]^2. \quad (2)$$

Where σ_{ij} is the estimated uncertainty in the *j-th* species *i-th* PM sample. For a properly assigned set of uncertainties the optimal Q should approach the theoretical degrees of freedom for factor analysis: $n \cdot m - p \cdot (m+n)$. Minimization of Eq. (2) is carried out using a Huber residual weighting so that results are robust to data outliers (Paatero, 1997, 1999; Reff et al., 2007).

The procedure of Polissar et al. (1998) was used to assign input data uncertainties in PMF3.0 — see also Reff et al. (2007). Data uncertainties (σ_{ij} in Eq. (2)) were computed as

$$\sigma_{ij} = \begin{cases} s_{ij} + DL/3, & if \quad X_{ij} > DL \\ 5 \cdot DL/6, & if \quad X_{ij} \leq DL \end{cases}. \quad (3)$$

Where s_{ij} is the laboratory analytical uncertainty for X_{ij} and DL is the detection limit value — estimated as three times the standard deviation of filter blank values. X_{ij} values below the detection limit (if any) were replaced by half of the DL value. We do not have missing values in the data sets analyzed.

Paatero et al. (2005) have shown how to graphically explore the range of potential solutions of Eq. (2) varying a parameter named *Fpeak*: positive values force most elements to lie on few source profiles, while negative values mean that most source profiles are mixed thus they do not stand for "pure sources"; they suggest varying *Fpeak* until correlation among paired source contributions $\{g_{ik}, g_{il}\}$ is minimized; this condition is graphically confirmed when several $\{g_{ik}, g_{il}\}$ points lay on either axis — the so called 'edge points' — and this means that k-th or l-th source is not contributing to PM mass on those data points; we follow that approach here.

3. Results and discussion

3.1. Mass concentration and chemical composition

For this campaign mean daily (24 h) concentrations of PM_{10} and $PM_{2.5}$ were 161 and 42 μg/m^3, respectively. The highest daily values were 331 μg/m^3 for PM_{10} and 108 μg/m^3 for $PM_{2.5}$; both happened the same day, December 29th 2007; the lowest measured values were 80 μg/m^3 for PM_{10} and 21 μg/m^3 for $PM_{2.5}$. Table 1 shows results for PM_{10} elemental concentrations measured with XRF — Na^+ and K^+ were measured by atomic absorption. The listed elements are the ones that had at most two values below the detection limit (DL) reported by the laboratory. The rightmost column in Table 1 has the DL value reported by the laboratory followed by the number of values below the DL, if any, between brackets. The species with the highest concentration is calcium, coming from the cement facility nearby — see Fig. 1 — and from suspended soil dust. Other species with high concentrations are silicon, sodium, iron, potassium and aluminum. Silicon and aluminum may come from cement manufacturing or suspended soil dust emissions. Potassium can be released from suspended soil dust and from specific processes such as the Li_2CO_3/KCl brine extraction plant located NNW of the monitoring site. Finally, sodium is assumed to come from marine aerosol reaching the monitoring site — see discussion below on wind trajectory analyses.

Table 1
Summary of chemical composition of ambient PM_{10}, in μg/m^3.

Species	Stand. dev.	Minimum	Mean	Median	Maximum	DL (# <)
Na^+	1.153	1.703	4.359	4.181	6.579	0.066
Al	0.363	0.995	1.602	1.637	2.231	0.014
Si	0.808	2.100	3.662	3.761	4.916	0.027
P	0.074	0.045	0.180	0.176	0.404	0.002
S	2.078	1.516	5.377	5.263	11.674	0.036
Cl	0.590	0.642	1.885	1.759	3.090	0.007
K	0.535	1.054	1.946	1.875	3.360	0.005
K^+	0.782	1.056	2.385	2.296	4.724	0.022
Ca	9.305	15.78	28.97	27.59	57.13	0.060
Ti	0.035	0.075	0.138	0.137	0.226	0.001
V	0.004	0.005	0.014	0.014	0.025	0.0001
Cr	0.001	0.000	0.004	0.004	0.007	0.001(1)
Mn	0.015	0.026	0.049	0.047	0.087	0.001
Fe	0.556	1.012	2.097	2.108	3.282	0.006
Ni	0.002	0.000	0.003	0.003	0.007	0.0003(2)
Cu	0.586	0.033	0.582	0.320	2.409	0.002
Zn	0.047	0.037	0.093	0.083	0.236	0.001
As	0.119	0.000	0.076	0.048	0.722	0.0002(1)
Br	0.005	0.006	0.014	0.013	0.026	0.001
Rb	0.004	0.005	0.011	0.010	0.025	0.001
Sr	0.013	0.017	0.038	0.037	0.068	0.001
Zr	0.003	0.001	0.007	0.007	0.014	0.002(2)
Pb	0.010	0.005	0.021	0.020	0.051	0.002

Table 2 shows a summary of species concentrations measured in the $PM_{2.5}$ fraction, using the same format as in Table 1. Species with higher concentrations are sulfates, calcium, organic and elemental carbon. Sulfates may come from primary emissions from cement kiln and copper smelter but may also be generated by the SO_X emissions from those sources through fast oxidation under favorable environmental conditions (see Fig. 2); calcium may come from the cement facility and suspended soil, and organic carbon and elemental carbon are tracers of combustion sources. Hence those four dominant species are all anthropogenic and the likely sources emitting them are the same ones already described for the PM_{10}.

Table 2
Summary of chemical composition of ambient $PM_{2.5}$, in μg/m^3.

Species	Stand. dev.	Minimum	Median	Mean	Maximum	DL (# <)
Al	0.117	0.087	0.216	0.224	0.722	0.006
Si	0.273	0.211	0.556	0.583	1.665	0.009
P	0.043	0.062	0.120	0.128	0.209	0.002
S	1.124	1.763	3.031	3.389	5.497	0.014
Cl	0.111	0.071	0.208	0.220	0.554	0.002
K	0.312	0.194	0.560	0.613	1.534	0.002
Ca	2.659	1.407	3.395	3.907	16.292	0.009
Ti	0.012	0.009	0.020	0.022	0.068	0.001
V	0.003	0.003	0.006	0.007	0.013	0.0001
Mn	0.004	0.002	0.009	0.010	0.025	0.0014
Fe	0.173	0.151	0.332	0.354	1.036	0.0025
Ni	0.001	0.000	0.002	0.002	0.007	0.0003(2)
Cu	0.043	0.017	0.058	0.068	0.212	0.0007
Zn	0.041	0.019	0.046	0.060	0.200	0.0007
As	0.080	0.003	0.029	0.050	0.476	0.0002
Br	0.001	0.002	0.004	0.004	0.007	0.0010
Rb	0.002	0.0005	0.003	0.004	0.010	0.0007(1)
Sr	0.004	0.002	0.006	0.007	0.019	0.0013
Pb	0.009	0.004	0.012	0.014	0.049	0.0018
NO_3^-	0.130	0.145	0.331	0.350	0.683	0.020
SO_4^{-2}	4.129	6.026	10.645	11.871	21.776	0.194
OC	0.766	1.552	2.494	2.645	5.314	0.228
EC	0.440	0.304	1.007	1.084	2.145	0.152
TC	1.005	1.856	3.676	3.728	5.777	0.253

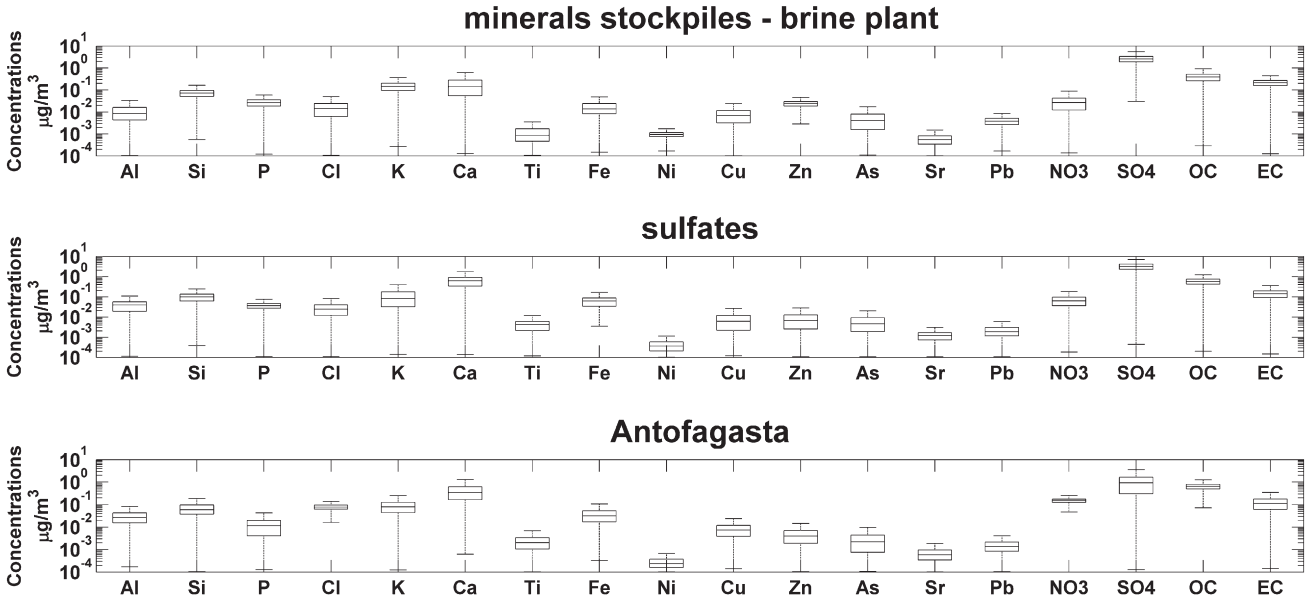

Fig. 2. Source profile concentrations [μg/m^3] for the six factor solution for ambient $PM_{2.5}$ (*Fpeak* = −0.05), factors 1–3.

3.2. Source apportionment for the PM_{10} fraction

Following the recommendations given in PMF3.0 User Guide (EPA, 2012) and in the technical literature (Reff et al., 2007), we have run the receptor model for $p = 3$, 4, and 5 factors including an additional, proportional model error originated from deviations from receptor model assumptions: source profile variability, potential sample contamination, etc. This additional model error was varied between 5 and 25% until the theoretical, a priori Q value $-n \cdot m - p \cdot (m+n)-$ was close to the *numerical* Q value out of the minimization of Eq. (2); this was achieved for an extra model uncertainty of 10%. Then we have applied Multiple Linear Regression (MLR) to the PM_{10} mass concentrations using the p source contributions as independent variables and checked whether MLR coefficients were positive and statistically significant ($p \leq 0.05$).

We have found that a five factor solution explains well measured PM_{10} concentrations. Elements fitted by PMF3.0 are: Al, Si, Cl, Ca, Ti, V, Mn, Fe, Ni, Cu, Zn, Br, Rb, Sr, Pb, Na^+ and K^+; all elements have regression coefficients (R^2) greater than 0.80, except two: V(0.73) and Ni(0.78). Kolmogorov–Smirnov test results support a Gaussian error distribution in model residues of all fitted species; all standardized residuals were lower than 3.0 except two: V(3.02) and Ni(−3.31). It was not possible to extract more sources out of this data set, as diagnosed by negative regression coefficients in the MLR of MP_{10} mass when six sources were chosen in PMF3.0.

Sensitivity analyses of this five factor solution were performed by applying the *Fpeak* parameter as described in the Methodology section. However we have found that the base simulation (*Fpeak* = 0) produced more plausible results.

Table 3 shows source profiles, in μg/m^3, and ratio of modeled to observed species concentrations for fitted species. All ratios are above 0.97 except Ni (0.83) showing a good model representation of elemental concentrations in ambient PM_{10} samples; Fig. 1 shows the variability in source profiles, computed using 1000 bootstrap runs. These results are discussed next.

The first source has more than 40% of the Al, Si, Ti, Mn, Fe and Sr measured; its K/Fe ratio is 0.66 so it corresponds to soil dust whose ratio is 0.6 ± 0.2 (Malm et al., 1994). The source profile shows a very stable composition of crustal elements; there is also chloride and sodium in this profile likely coming from marine aerosol deposition. The second source is identified as the cement manufacturing facility. It has the highest Ca concentration and bootstrap results for this profile shows narrow distributions for Ca, Al, Si, and Fe, all major components of cement; hence this stable source profile corresponds to the cement manufacturing facility which includes cement kiln and fugitive emissions from cement storing, handling and shipping.

Table 3
Source profiles for the five factor solution for PM_{10} fraction in μg/m^3 (*Fpeak* = 0).

Species	Soil dust	Cement plant	Copper smelter	Mineral stockpiles	Marine aerosol	Modeled conc.	Observed conc.	Ratio M/O
Al	0.6771	0.5355	0.1676	0.1926	0.0285	1.6012	1.6020	0.999
Si	1.5782	1.1685	0.3654	0.5130	0.0200	3.6450	3.6620	0.995
Cl	0.4530	0.4708	0.0031	0.2402	0.7000	1.8671	1.8850	0.990
Ca	10.3130	11.0410	4.1303	2.3434	0.7141	28.5418	28.9700	0.985
Ti	0.0551	0.0477	0.0153	0.0160	0.0031	0.1374	0.1380	0.995
V	0.0032	0.0049	0.0008	0.0026	0.0022	0.0135	0.0140	0.967
Mn	0.0190	0.0158	0.0069	0.0064	0.0004	0.0484	0.0490	0.988
Fe	0.8399	0.6652	0.2938	0.2612	0.0250	2.0850	2.0970	0.994
Ni	0.0000	0.0011	0.0000	0.0013	0.0001	0.0025	0.0030	0.831
Cu	0.0703	0.0021	0.3372	0.0387	0.1330	0.5813	0.5820	0.999
Zn	0.0099	0.0182	0.0120	0.0471	0.0048	0.0920	0.0930	0.989
Br	0.0035	0.0054	0.0011	0.0003	0.0034	0.0138	0.0140	0.989
Rb	0.0022	0.0055	0.0010	0.0012	0.0008	0.0107	0.0110	0.974
Sr	0.0149	0.0123	0.0060	0.0039	0.0000	0.0371	0.0380	0.978
Pb	0.0028	0.0023	0.0010	0.0107	0.0040	0.0207	0.0210	0.986
K^+	0.5516	1.1236	0.1503	0.2933	0.1995	2.3183	2.3850	0.972
Na^+	1.3220	1.0732	0.0801	0.5597	1.2928	4.3278	4.3590	0.993

Table 4
Source profiles for the six factor solution for $PM_{2.5}$ in μg/m^3 (*Fpeak* = −0.05).

Species	Mineral stockpiles & brine plant	Sulfates	Antofagasta	Copper smelter	Soil dust	Cement plant	Modeled conc.	Observed conc.	Ratio M/O
Al	0.002	0.036	0.025	0.013	0.051	0.096	0.222	0.224	0.989
Si	0.053	0.079	0.061	0.037	0.118	0.212	0.559	0.583	0.959
P	0.029	0.039	0.014	0.009	0.003	0.034	0.127	0.128	0.992
Cl	0.009	0.010	0.077	0.008	0.060	0.052	0.217	0.22	0.986
K	0.128	–	0.077	0.053	0.084	0.252	0.594	0.613	0.970
Ca	–	0.440	0.270	0.177	1.193	1.715	3.795	3.907	0.971
Ti	0.000	0.004	0.002	0.001	0.005	0.009	0.021	0.022	0.970
Fe	0.007	0.058	0.032	0.022	0.095	0.138	0.351	0.354	0.991
Ni	0.001	0.000	0.000	0.000	0.000	0.000	0.002	0.002	0.943
Cu	0.006	0.004	0.009	0.016	0.032	–	0.067	0.068	0.992
Zn	0.024	0.002	0.005	0.010	0.008	0.007	0.057	0.06	0.946
As	0.002	0.003	0.003	0.036	0.006	0.000	0.050	0.05	0.993
Sr	0.000	0.001	0.000	0.000	0.002	0.002	0.007	0.007	0.979
Pb	0.004	0.002	0.002	0.003	0.003	–	0.014	0.014	0.988
NO_3^-	0.025	0.069	0.153	0.018	0.004	0.081	0.348	0.35	0.995
$SO_4^=$	2.803	3.406	1.397	0.838	0.386	2.920	11.748	11.871	0.990
OC	0.461	0.606	0.712	0.074	0.248	0.414	2.515	2.645	0.951
EC	0.214	0.098	0.128	0.126	0.263	0.106	0.935	1.084	0.863

The third source has 58% of Cu, with a distinctively narrow concentration range so we identify it as the PM_{10} emission from the copper smelter, located ~3.7 km south of the monitoring site; the presence of crustal elements in this profile is an evidence of mixing of suspended soil dust emissions with the smelter plume en route to the monitoring site as shown by inspection of wind trajectories — see Discussion section below. Crustal element compositions also have a narrow concentration distribution but their average values are 2.5–4.3 times lower than in the soil dust profile.

The fourth source is identified with fugitive PM_{10} emissions from sulfide mineral stockpiles and from the brine plant. This source has ~51% of Zn, 53% of Ni and 52% of Pb, all tracers of sulfide ores (Fernández-Caliani et al., 2009) and that have stable concentrations in the source profile; the profile contains 13% of soluble potassium — a tracer of brine plant emissions — and also crustal elements but with lower concentrations than in the soil dust profile. The fifth source has 37.5% of Cl, 25% of Br and 30% of Na measured — all with narrow composition ranges distinctive of a stable source profile — so this is the marine aerosol. Crustal elements in this source profile have a broader composition distribution than in other source profiles and their average concentrations are 14 to 79 times lower than in the soil dust profile, showing a good source discrimination obtained by PMF3.0. Wind trajectory analysis confirms that this source is the marine aerosol and it may arrive to the monitoring site from different directions — see Discussion section below.

Table 5 shows results of the MLR of ambient concentrations of PM_{10} against source contributions; since the intercept is not statistically significant ($p = 0.062$), a MLR with a zero intercept was computed. The relative contributions to ambient PM_{10} and their standard deviations are: cement plant, 38.2 ± 1.5%; soil dust, 31.2 ± 2.3%; mineral stockpiles and brine plant, 12.7 ± 1.7%; copper smelter, 11.5 ± 1.6% and marine aerosol, 6.5 ± 2.4%. For this five factor solution a linear regression of modeled versus observed PM_{10} (not shown) explains 90% of the observed variance in ambient PM_{10}.

In the above analysis for PM_{10} sulfur was not considered because of its low R^2 value in model results when included as input to PMF3. As an ex post check we computed a MLR of sulfur concentrations using as independent variables the five $\{g_{ik}\}$ source contributions resolved with PMF3. The resulting sulfur apportionment equation is

$$S = 0.56 + 0.94G_1 + 1.78G_2 - 0.01G_3 + 1.36G_4 + 0.73G_5. \quad (4)$$

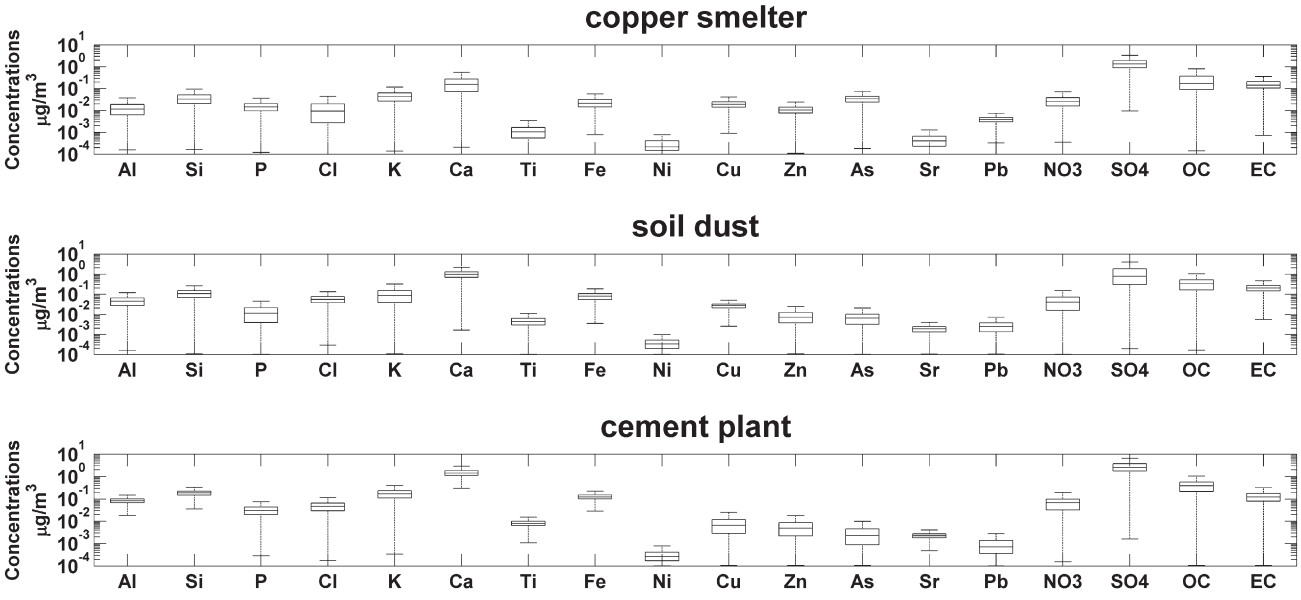

Fig. 3. Source profile concentrations [μg/m^3] for the six factor solution for ambient $PM_{2.5}$ (*Fpeak* = −0.05), factors 4–6.

Table 5
Summary of source apportionment results.

Source	MLR coefficient ($\mu g/m^3$)	Standard error ($\mu g/m^3$)
PM_{10}		
Soil dust	50.3	3.8
Cement plant	61.6	2.4
Copper smelter	18.5	2.5
Mineral stockpiles & lithium/KCl plant	20.4	2.7
Marine aerosol	10.4	3.9
$PM_{2.5}$		
Mineral stockpiles & lithium/KCl plant	5.15	0.49
Sulfates	7.43	0.71
Antofagasta	3.53	0.56
Copper smelter	2.19	0.32
Soil dust	9.32	0.69
Cement plant	14.05	0.52

This result shows that sulfur is apportioned to all sources but the copper smelter and in similar amounts ~1 $\mu g/m^3$, so its contribution to most source profiles is relevant; the above results in Eq. (4) confirm the source identification already obtained for PM_{10}. Nonetheless, we do get a low R^2 in the above equation (0.39, adjusted value) so we chose not to include sulfur in the final model.

We now comment on our choice of soluble potassium — measured by ionic chromatography — in place of total potassium — as measured by XRF — in the receptor model analysis for PM_{10}. A reduced major axis regression applied to those paired data showed consistence among them ($R^2 = 0.88$) and both measurements produced nearly the same fitting R^2 values in PMF3: 0.97 for K^+ and 0.94 for K. A MLR of potassium concentrations against the five $\{g_{ik}\}$ source contributions produced results similar to the ones shown in Table 3 for K^+. Hence model receptor results are equivalent for either choice of input measurements.

3.3. Source apportionment for the fine fraction ($PM_{2.5}$)

PMF3.0 was run for $p = 4$, 5 and 6 factors, and we have found that a six factor solution describes well $PM_{2.5}$ ambient concentrations; an extra modeling uncertainty of 11% produces a numerical Q value close to the theoretical one. The fitted species are: Al, Si, P, Cl, K, Ca, Ti, Fe, Ni, Cu, Zn, As, Sr, Pb, NO_3^-, SO_4^{-2}, organic (OC) and elemental carbon (EC). Most fitted species had correlation coefficients higher than 0.84; the exceptions are OC (0.48) and EC (0.49) that were kept in the final solution for they are tracers that help identify sources. Kolmogorov–Smirnov test results support a Gaussian error distribution in model residues for all fitted species; only two standardized residues were higher than 3.0: K (3.39) and Zn (3.37).

For this data set sulfur and sulfate were highly correlated; a reduced major axis regression of these paired data has $R^2 = 0.96$. In Table 4 sulfates have a fitting $R^2 = 0.99$, slightly better than in the case of sulfur ($R^2 = 0.97$) obtained by MLR of sulfur concentrations against the six source contributions $\{g_{ik}\}$. Given this equivalence, we have chosen sulfates as input to PMF3 in the source apportionment of $PM_{2.5}$.

Sensitivity analyses of this six factor solution were performed by applying the *Fpeak* parameter. For this fine fraction we have found that the better source identification was achieved by using *Fpeak* = −0.05, so this one is presented in this work. Table 4 shows source profiles and ratio of modeled to observed concentration for fitted species. All ratios are between 0.94 and 1.0 — except for EC (0.86) — showing a good model representation of measured species concentrations in ambient $PM_{2.5}$ samples. Figs. 2 and 3 show the variability in source profiles, computed using 1000 bootstrap runs in PMF3. These results are discussed next.

The first source has more than 50% of Ni, 40% of Zn and 28% of Pb, all with narrow concentration range in the source profile so it corresponds to fugitive $PM_{2.5}$ from mineral stockpiles 12 km NNE of the monitoring site; this source also has 24% of sulfates, 23% of EC, 21% of potassium and 18% of OC showing enrichment with particle deposition from cement kiln, copper smelter and brine plant emissions as well. The second source has 29% of sulfates, 30% of P, 24% of OC and 10.5% of EC, all with narrow concentration ranges so it is a sulfate plume originated from copper smelter emissions. The ratio S/P ~ 30 in this profile is similar to values obtained for copper smelter contributions to ambient $PM_{2.5}$ at Santiago (Rojas et al., 1990; Jorquera and Barraza, 2012).

The third source has the highest concentrations of chlorine, nitrate and OC which show a stable source profile hence it comes from combustion sources and it is a plume aged enough to have nitrates within; thus we identify it as the plume of Antofagasta moving inland; the

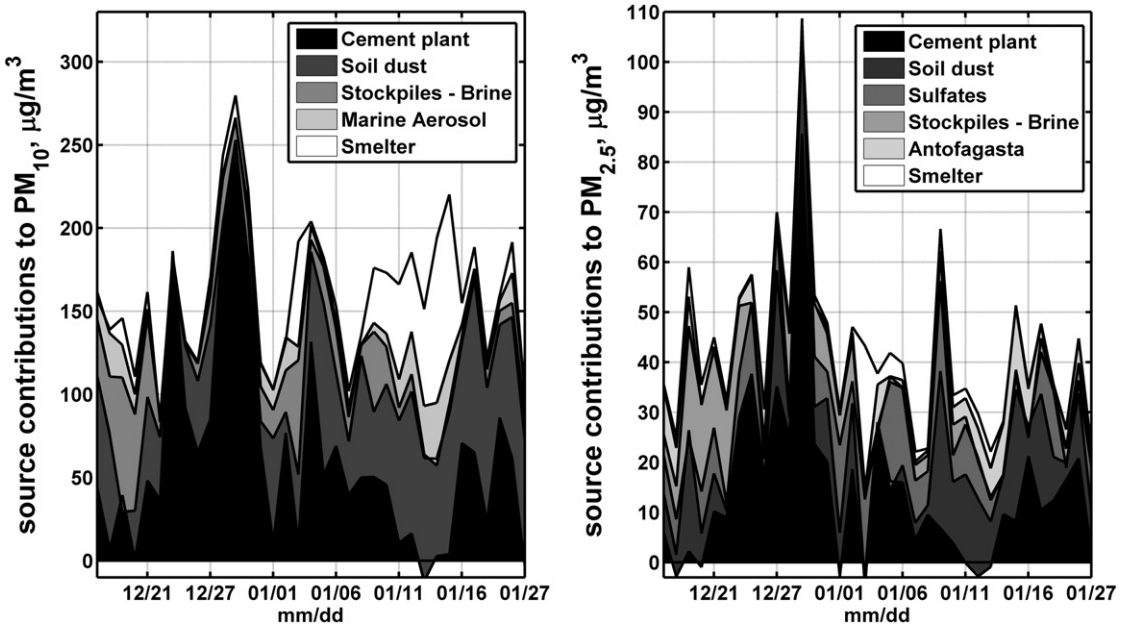

Fig. 4. Time series plots of source contributions to PM_{10} and $PM_{2.5}$ concentrations, in [$\mu g/m^3$].

anthropogenic origin is also supported by a ratio K/Fe = 2.4. This source includes emissions from vehicular traffic and shipping activities at Antofagasta; the presence of chlorine in this source profile is due to mixing of marine aerosol as air masses move from the coast towards the monitoring site. Nonetheless, secondary and carbonaceous aerosols dominate in this profile so we identify this source as the contribution to $PM_{2.5}$ from Antofagasta. Furthermore, this source is different from the marine aerosol source profile identified in the PM_{10} fraction that is dominated by sea salt (see Table 3).

The fourth source has more than 70% of As, and it has 24% of Cu and Pb and 18% of Zn, all tracers of primary copper smelter emissions (Hedberg et al., 2005) that have small composition variability in the source profile. The fifth source has crustal species such as Al, Si, K, Ca, Ti, Fe and Sr with small composition variability in the source profile; the ratio K/Fe = 0.88 supports that this source is the suspended soil dust; there is a clear enrichment of this source profile with Cl, K and Cu deposited on the ground and accumulated in this desert region. The sixth source has more than 45% of Ca; species such as Al, Si, Ca Fe, sulfates and OC have small composition variability in the source profile. Furthermore the ratios Ca/Fe = 12.5 and $Ca/SO_4^{-2} = 0.59$ are characteristic of cement kiln emissions (Chow et al., 2004) thus this is the cement plant source.

A MLR analysis was carried out with ambient $PM_{2.5}$ concentrations and source contributions from the six sources identified. Once again, the intercept was not significant ($p = 0.85$), so a MLR with zero intercept produced the source contributions shown in Table 5. The relative contributions to ambient $PM_{2.5}$ concentrations and their standard errors are: cement plant: 33.7 ± 1.3%, soil dust: 22.4 ± 1.6%, sulfates: 17.8 ± 1.7%, mineral stockpiles and brine plant: 12.4 ± 1.2%, Antofagasta: 8.5 ± 1.3% and copper smelter: 5.3 ± 0.8%. For this six factor solution a linear regression of modeled versus observed $PM_{2.5}$ (not shown) explains 95% of the variance observed in ambient $PM_{2.5}$.

4. Discussion

Fig. 4 shows time series plots of $PM_{2.5}$ and PM_{10} source contributions for the period of the measurement campaign. In some days the receptor model predicts negative contributions from one or two sources, but total model estimation is quite close to measured concentrations. On December 29th ambient PM_{10} reached a peak of 331 μg/m^3 and the receptor model estimated a value of 280 μg/m^3; for the $PM_{2.5}$ fraction the peak measured value was 108 μg/m^3 and the model predicted 107 μg/m^3.

In order to confirm source identification we have conducted an analysis of wind trajectories, using the Hybrid Single-Particle Lagrangian Integrated Trajectory (HYSPLIT) from the USA's National Oceanic and Atmospheric Administration, NOAA (Rolph, 2012). We have constructed 24 h monitor-backward and source-forward trajectories to check receptor model results; the NCEP meteorological database has been chosen with an explicit modeling of the vertical wind velocity and initial trajectories have been set at 100 m above ground level. Using this methodology we have found that:

a) The highest soil dust contributions to PM_{10} and $PM_{2.5}$ happen when wind direction is S–SSW–SW and soil dust is mixed with marine aerosol and copper smelter emissions — see Fig. 5, Supplementary material for January 15th.
b) When W–WNW winds enter Antofagasta's basin they move towards the monitoring site bringing in contributions from Antofagasta, soil dust and cement plant emissions — see Fig. 5 for January 17th.

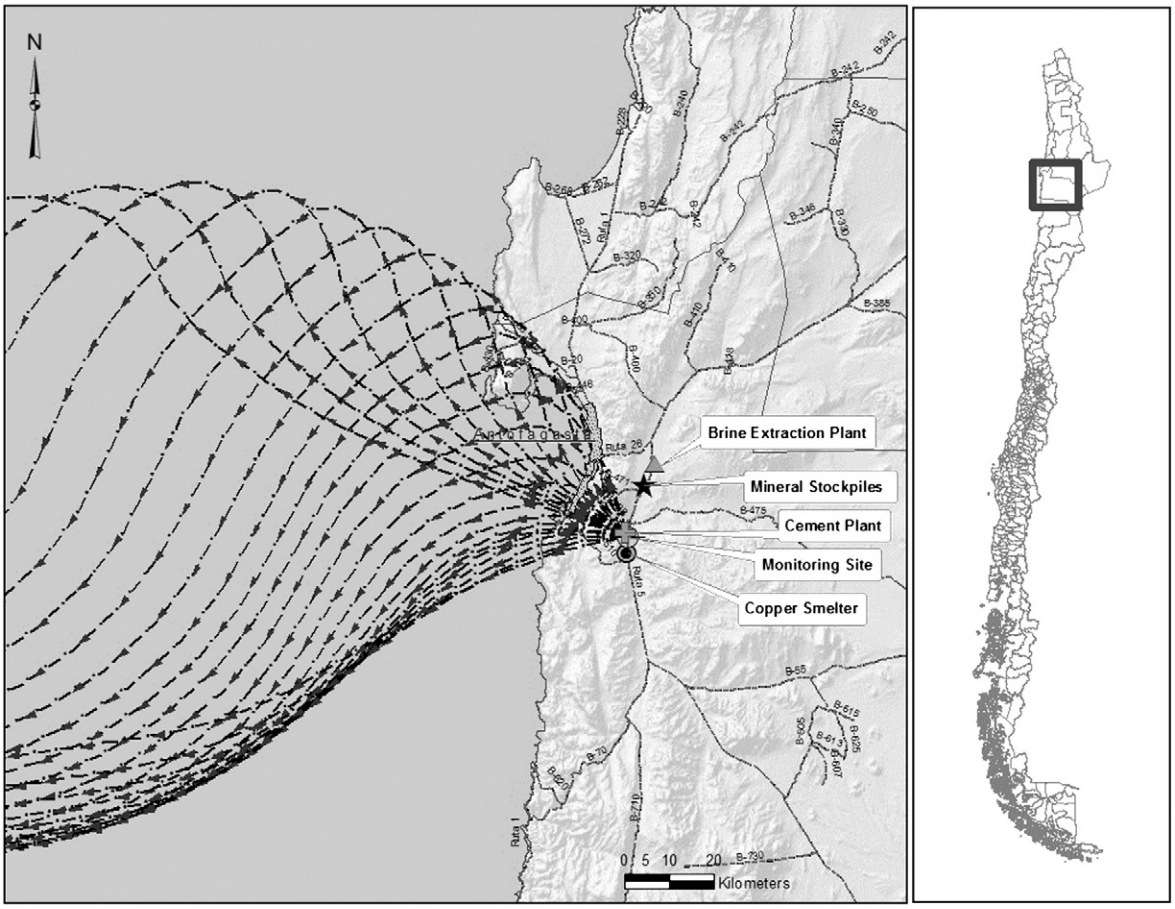

Fig. 5. Backward trajectories arriving at the monitor site on January 17th, 2008.

c) When wind trajectories directly go from a source towards the monitor, the impacts of such source on measured values are the highest and this is consistent with the outcomes of the receptor modeling analysis for the very same day. For instance, this happens for the cement plant emissions in December 29th (Fig. 6, Supplementary material) when the highest values of PM_{10} and $PM_{2.5}$ were recorded, for the mineral stockpiles and brine plant emissions on December 19th — see Fig. 6 — and for the copper smelter on January 3rd (Fig. 7, Supplementary material) when the highest values of As were recorded in both PM size fractions.

We acknowledge that wind trajectory analyses may not be accurate when terrain features like the coastal range are present. Hence we have checked the above analysis using the local wind measured at the monitoring site for the campaign period. We show in Fig. 7 compass plots for December 19th and January 17th; it can be seen that in December 19th there were five hours when wind direction was between 30 and 60°, that is, from the location of the minerals stockpiles and the brine plant towards the monitoring site; likewise in January 17th there were nine hours with wind direction between 270 and 300° thus bringing contributions from Antofagasta and cement plant emissions to the monitoring site. Therefore, local wind data in Fig. 7 are in agreement with the wind trajectories shown in Figs. 5 and 6.

Inspection of correlation coefficients among $\{g_{ik}\}$ source contributions to $PM_{2.5}$ shows that sulfate contributions are significantly correlated with the copper smelter and Antofagasta contributions ($p<0.05$); there is a negative — but not statistically significant ($p=0.14$) — correlation between sulfates and cement plant contributions. In addition, the ratio S/P~30 in the sulfates source profile (Table 4) is similar to values obtained for copper smelters contributions to ambient $PM_{2.5}$ at Santiago (Rojas et al., 1990; Jorquera and Barraza, 2012). Hence results suggest that sulfates in the $PM_{2.5}$ fraction come mostly from the copper smelter emissions either as directly emitted sulfates or produced by the oxidation of SOx emissions from that source.

One source that appears in $PM_{2.5}$ but not in PM_{10} is Antofagasta; this source was characterized by high contents of carbonaceous and secondary aerosols (Table 4), species that were only measured in the $PM_{2.5}$ fraction. On the other hand marine aerosol is resolved in the PM_{10} (Table 3) but not as a single source in the $PM_{2.5}$ analysis; this result is probably due to the small sample size analyzed with PMF3.

The anthropogenic source that contributes most at the PM_{10} size fraction is the cement plant, followed by mineral stockpiles–brine plant and the copper smelter source. For the $PM_{2.5}$ fraction the relative order is cement plant, copper smelter (including sulfates) and mineral stockpiles–brine plant sources; so most pollution come from local sources and not from regional ones. Values of the soil dust contribution are higher than those estimated at other locations in the same region — see Introduction section — and we ascribe this result to the bare landscape in the study area as compared with urbanized ground landscapes for the cities mentioned in the Introduction section.

The model receptor analysis shows that suspended soil dust is enriched with elements of natural and anthropogenic origin: sodium chloride from marine aerosol, Ca and sulfates from the cement plant, Cu, Zn, As and sulfates from the copper smelter, Zn, Pb, S and Ni from the mineral stockpiles; all these elements deposit and accumulate on the ground due to the lack of precipitation in this desert region and are easily suspended by the local winds therein — see Fig. 4, Supplementary material; these soil dust accumulation and suspension

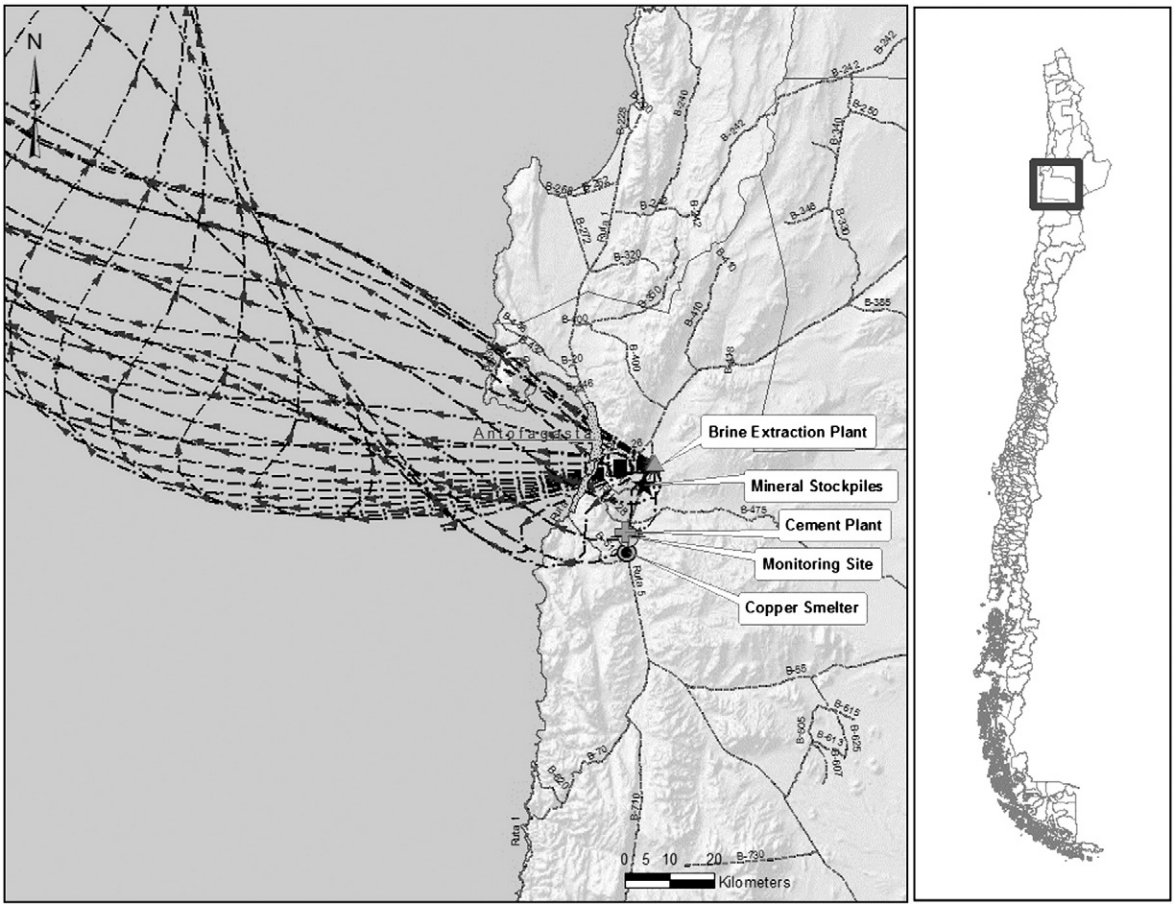

Fig. 6. Forward wind trajectories departing from the brine plant on December 19th, 2007.

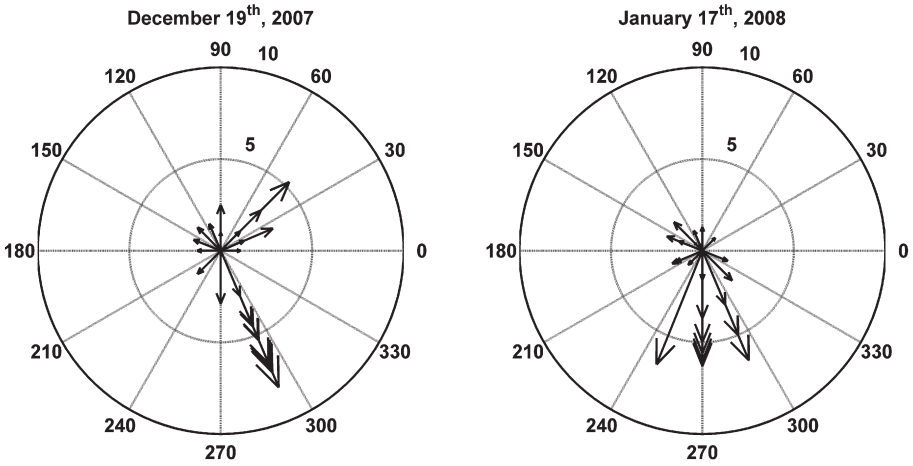

Fig. 7. Compass plots of local wind data for December 19th, 2007 and January 17th, 2008.

mechanisms are difficult to be modeled using source-oriented dispersion models. Anthropogenic sources such as copper smelter, cement plant and minerals stockpile emissions get mixed with suspended soil dust at the monitoring site. Wind trajectory analyses and inspection of local winds have confirmed such interpretation — see Figs. 5–7 and those in the Supplementary material.

5. Conclusions

A short term campaign measuring chemical speciation in ambient PM_{10} and $PM_{2.5}$ size fractions was conducted between December 17th, 2007 and January 27th, 2008 near Antofagasta, a mid-size coastal city in northern Chile. The site is within a desert that includes northern Chile and most of southwestern Perú.

Source apportionment was estimated by applying U.S. EPA's Positive Matrix Factorization receptor modeling software — version 3.0 — to PM_{10} and $PM_{2.5}$ size fractions. Sources were identified by inspection of source profiles for key tracers, tracer ratios, local winds and wind trajectory analyses. The relative contribution results for the $PM_{2.5}$ fraction are: cement plant: $33.7 \pm 1.3\%$, soil dust: $22.4 \pm 1.6\%$, sulfates: $17.8 \pm 1.7\%$, minerals stockpiles/brine plant: $12.4 \pm 1.2\%$, Antofagasta: $8.5 \pm 1.3\%$ and copper smelter: $5.3 \pm 0.8\%$. For the PM_{10} fraction the contributions are: cement plant, $38.2 \pm 1.5\%$; soil dust, $31.2 \pm 2.3\%$; sulfide stockpiles/brine plant, $12.7 \pm 1.7\%$; copper smelter, $11.5 \pm 1.6\%$ and marine aerosol, $6.5 \pm 2.4\%$. Hence local sources contribute to ambient PM concentrations more than distant sources (Antofagasta, marine aerosol) do.

Suspended soil dust has a mean contribution of 50 $\mu g/m^3$ to ambient PM_{10} and its peak daily value is 104 $\mu g/m^3$. For the fine fraction, the contributions are 9.3 $\mu g/m^3$ and 31.5 $\mu g/m^3$, respectively.

Supplementary data to this article can be found online at http://dx.doi.org/10.1016/j.scitotenv.2012.12.007.

Acknowledgments

Financial support for this work was provided by the Industria Nacional de Cemento S.A.; the company also provided access to installing ambient samplers. We thank Mrs. Yolanda Silva (www.setec.cl) for conducting the ambient monitoring sampling and Mr. Steven Kohl for the chemical analyses performed at the Desert Research Institute (www.dri.edu). We acknowledge a CONICYT doctoral fellowship granted to one of us (F. Barraza). The research described in this article has not been subjected to any review by the funding institutions thus no official endorsement should be inferred.

References

Chow JC, Watson JG, Kuhns H, Etyemezian V, Lowenthal DH, Crow D, et al. Source profiles for industrial, mobile, and area sources in the Big Bend Regional Aerosol Visibility and Observational study. Chemosphere 2004;54:185–208.
COCHILCO. Statistics on Chilean and worldwide copper production. can be downloaded from http://www.cochilco.cl/productos/base_datos.asp 2012. [Accessed August 2012].
Fernández-Caliani JC, Barba-Brioso C, González I, Galán E. Heavy metal pollution in soils around the abandoned mine sites of the Iberian pyrite belt (southwest Spain). Water Air Soil Pollut 2009;200:211–26.
Fiebig-Wittmaack M, Schultz E, Cordova AM, Pizarro C. A microscopic and chemical study of airborne coarse particles with particular reference to sea salt in Chile at 30° S. Atmos Environ 2006;40:3467–78.
Hedberg E, Gidhagen L, Johansson C. Source contributions to PM10 and arsenic concentrations in Central Chile using positive matrix factorization. Atmos Environ 2005;39:549–61.
Hopke PK, et al. PM source apportionment and health effects: 1. Intercomparison of source apportionment results. J Expo Anal Environ Epidemiol 2005;1:1-12.
Jorquera H. Source apportionment of PM_{10} and $PM_{2.5}$ at Tocopilla, Chile (22°05′S, 70°12′W). Environ Monit Assess 2009;153:235–51.
Jorquera H, Barraza F. Source apportionment of ambient $PM_{2.5}$ in Santiago, Chile: 1999 and 2004 results. Sci Total Environ 2012;435–436:418–29.
Kavouras I, Koutrakis P, Cereceda-Balic F, Oyola P. Source apportionment of PM_{10} and $PM_{2.5}$ in five Chilean cities using factor analysis. J Air Waste Manage Assoc 2001;51:451–64.
Malm WC, Sisler JF, Huffman D, Eldred RA, Cahill TA. Spatial and seasonal trends in particle concentration and optical extinction in the United States. J Geophys Res 1994;99(D1):1347–70.
Mansbach DK, Norris JR. Low-level cloud variability over the equatorial cold tongue in observations and models. J Climate 2007;20:1555–70.
National System of Air Quality Monitoring Information SINCA. Data available for download at http://sinca.mma.gob.cl 2012. [Accessed August 2012].
Okin GS, Bullard JE, Reynolds RL, Ballantine JAC, Schepanski K, Todd MC, et al. Dust: small-scale processes with global consequences. EOS Trans Am Geophys Union 2011;92(29):241–2. 19th July, Available from www.agu.org. Accessed August 2012.
Paatero P. Least squares formulation of robust nonnegative factor analysis. Chemom Intell Lab Syst 1997;37:23–35.
Paatero P. The multilinear engine — a table-driven, least squares program for solving multilinear problems, including the n-way parallel factor analysis model. J Comput Graph Stat 1999;1:854–88.
Paatero P, Hopke PK, Begum BA, Biswas SK. A graphical diagnostic method for assessing the rotation in factor analytical models of atmospheric pollution. Atmos Environ 2005;39:193–201.
Pant P, Harrison RM. Critical review of receptor modelling for particulate matter: a case study of India. Atmos Environ 2012;49:1-12.
Polissar AV, Hopke PK, Paatero P, Malm WC, Sisler JF. Atmospheric aerosol over Alaska: 2. Elemental composition and sources. J Geophys Res 1998;103(D15):19045–57.
Reff A, Eberly SI, Bhave PV. Receptor modeling of ambient particulate matter data using positive matrix factorization: review of existing methods. J Air Waste Manage Assoc 2007;57:146–54.
Rojas CM, Artaxo P, Van Grieken R. Aerosols in Santiago de Chile: a study using receptor modeling with X-ray fluorescence and single particle analysis. Atmos Environ Part B Urban Atmos 1990;24:227–41.
Rolph GD., 2012 Real-time Environmental Applications and Display System (READY) Website (http://ready.arl.noaa.gov). NOAA Air Resources Laboratory, Silver Spring, MD.
Sun R, Moorthi S, Xiao H, Mechoso CR. Simulation of low clouds in the Southeast Pacific by the NCEP GFS: sensitivity to vertical mixing. Atmos Chem Phys 2010;10:12261–72.
U.S. Environmental Protection Agency. PMF3.0 Software and User Guide. available from http://www.epa.gov/heasd/products/pmf/pmf.html 2012. [Accessed: August 2012].
Xu H, Xie S-P, Wang Y. Subseasonal variability of the southeast Pacific stratus cloud deck. J Climate 2005;18:131–42.